Article (Discoveries)

Correlated evolution of large DNA fragments in the chromatin interaction network: a case study in *Arabidopsis thaliana*

Yubin Yan[†,1], Zhaohong Li[†,1], Ye Li[1], Zefeng Wu[1], Ruolin Yang[*,1]

[1]College of Life Sciences, Northwest A&F University, Yangling, Shaanxi, China

[†]These authors contributed equally to this work.

[*]Corresponding author: Email: desert.ruolin@gmail.com.

Abstract

In eukaryotes, the three-dimensional (3D) conformation of the genome is far from random, and this nonrandom chromatin organization is strongly correlated with gene expression and protein function, which are two critical determinants of the selective constraints and evolutionary rates of genes. However, whether genes and other elements that are located close to each other in the 3D genome evolve in a coordinated way has not been investigated in any organism. To address this question, we constructed chromatin interaction networks (CINs) in *Arabidopsis thaliana* based on high-throughput chromosome conformation capture (Hi-C) data and demonstrated that adjacent large DNA fragments in the CIN indeed exhibit more similar levels of polymorphism and evolutionary rates than random fragment pairs. Using simulations that account for the linear distance between fragments, we proved that the 3D chromosomal organization plays a role in the observed correlated evolution. Interacting Hi-C fragments also exhibit more similar mutation rates and functional constraints in both coding and noncoding regions than the random expectations, indicating that the coordinated evolution between 3D neighbors is a result of combined evolutionary forces. A collection of 39 genomic and epigenomic features can explain much of the variance in genetic diversity and evolutionary rates across the genome. Moreover, features that have a greater effect on the evolution of regional sequences tend to show higher similarity between neighboring fragments in the CIN, suggesting a pivotal role of epigenetic modifications and chromatin organization in determining the correlated evolution of large DNA fragments in the 3D genome.

Keywords: correlated evolution, 3D genome, chromatin interaction network, *Arabidopsis thaliana*, population genetics

Introduction

At all levels of the hierarchical organization of living systems, biological units rarely evolve in isolation. For instance, species interact with each other in various ways, such as parasitism, competition, and mutualism. Within organisms, proteins encoded by different genes of the same genome or different genomes (i.e., the nuclear and cytoplasmic genomes) frequently act together to accomplish specific functions. When two or more evolving units interact and produce reciprocal evolutionary changes in each other, we say there is coevolution between them (Carmona et al. 2015). At the species level, a change in one species may impose evolutionary pressure on its interacting species, giving rise to reciprocal modifications in these organisms, as observed in host-pathogen and pollinator/herbivore-plant coevolution (Ehrlich and Raven 1964; Burdon and Thrall 2009). At the molecular level, a mutation that disrupts the structure and function of a protein or a tRNA may be compensated by a second mutation in the same molecule, resulting in no deleterious effect of the first mutation (Kondrashov et al. 2002; Kern and Kondrashov 2004). Such compensatory mutations can occur between interacting molecules as well, leading to molecular coevolution between different molecules (Pazos and Valencia 2008).

Compensatory coevolution at the molecular level may result in correlated evolutionary rates and similar phylogenetic profiles between interacting proteins. Many methods have been developed for detecting protein coevolution based on principles of molecular phylogenetics, and the coevolutionary pattern between residues has been used to predict protein structure and novel interactions [see de Juan et al. (2013) for a review]. In addition to the similarity in phylogenetic profiles, correlated evolutionary rates have been regarded as one of the consequences of compensatory coevolution and have been widely observed between interacting proteins. For example, accelerated rates of evolution in nuclear genes that cooperate with mitochondrial genes

have been reported in many animal species (Osada and Akashi 2012; Barreto and Burton 2013; Parmakelis et al. 2013; Barreto et al. 2018), possibly as a result of the high mutation rate in the mitochondrial genome and the accumulation of compensatory mutations in the nuclear genes (Rand et al. 2004; Levin et al. 2014; Sloan et al. 2018). Such accelerated compensatory coevolution has been observed in some plants with elevated mutation rates in the plastid genome as well (Zhang et al. 2015; Weng et al. 2016). The correlation of evolutionary rates between interacting genes is evident even at the whole-interactome level in an organism (Fraser et al. 2002; Alvarez-Ponce and Fares 2012).

It should be noted, however, that not all of the correlation of evolutionary rates between interacting genes can be attributed to the coevolutionary process. Interacting proteins are usually involved in related biological functions and exhibit comparable expression patterns, which will lead to similarity in the selective pressure exerted on the proteins and give rise to the observed correlated evolutionary rate (Juan et al. 2008). In any case, an analysis of correlated evolution between interacting genes or other evolving units will provide insights into the organization and functionality of living organisms, whether the covariation derives from similar selective pressure or reciprocal evolutionary changes.

As mentioned above, correlated evolution and coevolution at the molecular level have been extensively studied, focusing mostly on functional genes in the genome. With the advance of chromosome conformation capture (3C) and its high-throughput derivate (i.e., Hi-C) technique (Lieberman-Aiden et al. 2009) during the last decade, another type of interaction, the physical contact of genomic DNA in the nucleus, has been revealed at the whole-genome scale with an unprecedented resolution in many organisms. Similar to gene arrangement at the linear level, the 3D organization of the genome in the nucleus is far from random. In eukaryotes, chromosomes

are arranged into discrete territories and other finer structures (e.g., A/B compartments, topologically associated domains, chromatin loops), and this architecture influences many biological activities such as gene transcription and splicing (Bonev and Cavalli 2016; Ruiz-Velasco and Zaugg 2017). Recent studies based on Hi-C data have shown that genes that are in direct contact in the 3D space of the nucleus tend to be coexpressed (Ben-Elazar et al. 2013; Homouz and Kudlicki 2013; Ay, Bunnik, et al. 2014; Babaei et al. 2015) and to present comparable biological functions based on different measurements of functional similarity (Homouz and Kudlicki 2013; Diament et al. 2014). In addition, fragments in physical contact in the 3D genome exhibit more correlated mutations (Perlaza-Jimenez and Walther 2018), suggesting functional interaction between 3D neighbors. Because expression level/breadth and functional constraints are two important predictors of the evolutionary rate of protein-coding genes (Pal et al. 2006; Zhang and Yang 2015), we expect that interacting genes in the 3D chromatin network will evolve in a coordinated fashion. However, to our knowledge, such a hypothesis has not been explicitly tested in any species. Furthermore, considering that interacting DNA fragments in the nucleus contain a substantial proportion of noncoding sequences, do these sequences subjected to lower levels of selective pressure also evolve in a coordinated way?

Here, we explicitly tested the hypothesis that genes and other noncoding sequences located nearby in the 3D genome evolve in a coordinated manner using *Arabidopsis thaliana* as a case study. Specifically, we constructed chromatin interaction networks (CINs) with Hi-C datasets from multiple sources at different resolutions in *A. thaliana* and compared the similarity of genetic diversity and evolutionary rates between 3D neighboring fragments with the random expectation. We aimed to answer the following questions: 1). Do genetic fragments that interact at the 3D scale evolve in a coordinated manner in terms of genetic diversity and evolutionary

rate? 2). If so, what evolutionary forces have driven the observed pattern? Do fragments located close to each other in the 3D structure exhibit comparable mutation rates? Have they experienced similar evolutionary pressures? Do interacting elements coadapt to each other, resulting in a pattern of coevolution?

In addition, it is known that chromatin organization and other genomic features (e.g., GC content, recombination rates, and replication timing) influence the regional mutation rate in both germline and somatic cells (Stamatoyannopoulos et al. 2009; Schuster-Bockler and Lehner 2012; Woo and Li 2012; Segurel et al. 2014; Makova and Hardison 2015) and, hence, affect local genetic diversity and evolutionary rates. With the availability of a plethora of functional genomic and epigenomic data in the model species Arabidopsis, we are able to comprehensively explore the relationships between various genomic and epigenomic features and different evolutionary forces (e.g., mutation rates, natural selection), along with their implications for the correlated evolution of 3D neighboring fragments.

Results

Neighboring fragments in the CIN show similar levels of nucleotide diversity and evolutionary rates

We constructed a CIN with both significant intra- and inter-chromosomal contacts at a 100 kb resolution using Hi-C data from Liu et al. (2016) and Wang et al. (2015). Because some of our analyses require a large number of sites from particular categories (e.g., 0-fold and 4-fold degenerate sites) within a single fragment to obtain reliable results, we retained only individual windows with more than 15 protein-coding genes where more than 20% of the sequences could

be reliably aligned to *A. lyrata* (see Materials and Methods). For each of the remaining 100 kb nonoverlapping windows, we calculated the average nucleotide diversity (π) based on biallelic SNPs in a global Arabidopsis collection (Alonso-Blanco et al. 2016) and the evolutionary rate based on the divergence between *A. thaliana* and *A. lyrata* at alignable sites. Both genetic diversity and evolutionary rates vary greatly within the genome, with nucleotide diversity showing greater variance (CV = 43.7% and 17.8% for diversity and divergence, respectively; supplementary fig. S1). Among the different classes of nucleotides, 0-fold degenerate sites present the lowest levels of genetic diversity and lowest evolutionary rate, while 4-fold degenerate sites and putatively neutral noncoding sequences (NNSs; see definition in the Materials and Methods) exhibit much higher polymorphism and evolve much faster, and putatively functional noncoding sites [defined as conserved noncoding sequences identified in Haudry et al. (2013) plus UTRs, hereafter abbreviated as CNS+UTR] show intermediate diversity and divergence (supplementary fig. S2; supplementary table S1). This is consistent with the different levels of selective constraints acting on putatively functional and neutral sites.

As observed in other types of interaction networks (Fraser et al. 2002; Alvarez-Ponce and Fares 2012), fragments with more connections in the CIN might be subjected to a higher level of selective constraint, as reflected by a strong negative correlation between the node degree and mean diversity (fig. 1A; Pearson's correlation coefficient: $r = -0.46$; P-value $< 2.2 \times 10^{-16}$) and a significant positive correlation between the node degree and the proportion of SNPs with a derived allele frequency of less than 0.5% [%(DAF < 0.005); fig. 1B; $r = 0.43$; $P < 2.2 \times 10^{-16}$]. Highly connected fragments also tend to evolve more slowly than those exhibiting fewer connections (fig. 1C; $r = -0.53$; $P < 2.2 \times 10^{-16}$). There is a significant positive correlation between the node degree and the number of genes within fragments (fig. 1D; $r = 0.52$; $P < 2.2 \times$

10^{-16}), which may explain the correlation between the degree centrality and selective constraints. However, the results of partial correlation analyses show that the number of genes within fragments cannot fully explain the observed pattern; after accounting for the variation of gene numbers, the correlation coefficients between the node degree and diversity, %(DAF < 0.005), and divergence are -0.36, 0.36, and -0.41, respectively ($P = 5.0 \times 10^{-30}$, 5.6×10^{-31}, and 6.4×10^{-40}, respectively).

To test whether large DNA fragments that are in contact in the 3D space evolve in a coordinated fashion, we compared the observed average differences in nucleotide diversity and evolutionary rates between immediate neighbors in the CIN to those in different null models. In the first model, we rewired the graph while the degree distribution was preserved. For both polymorphism and divergence, the observed difference between fragments in contact is significantly smaller than that of the random network (P-value < 0.001 for both polymorphism and divergence; supplementary fig. S3), suggesting that neighboring fragments in the 3D genome indeed evolve in a coordinated way. Since DNA fragments that are in proximity at the linear scale tend to be neighbors in the 3D space as well and physically linked genes tend to be coexpressed (Boutanaev et al. 2002; Williams and Bowles 2004) and evolve at similar rates (Williams and Hurst 2000), the detected similarity may be a product of one-dimensional organization of the genome. To test whether the 3D arrangement of DNA in the nucleus contributes to the observed correlated evolution, we performed a more conservative simulation, a cyclic chromosome shift (CCS) model (Diament et al. 2014), in which the linear adjacency among fragments is preserved along their "circular" chromosomes, while their 3D interacting relationship is perturbed (see Materials and Methods). The differences in genetic diversity and evolutionary rates in the real data are still significantly smaller than those in the simulated

networks (P-value < 0.001 in both cases; fig. 2A, B). This conclusion also holds under the cyclic genome shift model, which is similar to the CCS model but allows fragments to rotate and move between different chromosomes (supplementary fig. S4). In the following sections, we present only the results of the CCS simulations because they are the most appropriate null models for testing the effects of 3D organization on the correlated evolution between Hi-C contacting fragments.

Furthermore, the similarities in nucleotide diversity and evolutionary rates between fragment pairs both decrease with an increase in topological distance in the CIN (fig. 2C, D). These results indicate that the large fragments containing genes and other DNA elements are arranged in a nonrandom manner in Arabidopsis and that 3D chromatin organization contributes to the correlated evolution of genetic elements that are close to each other in higher dimensional space. The pattern of correlated evolution between 3D neighbors is retained when we use another independent Hi-C dataset derived from four-week-old rosette leaves in Arabidopsis (Feng et al. 2014) (supplementary fig. S5).

Evolutionary forces that contribute to the correlated evolution between 3D chromatin neighbors: mutation rate

The levels of genetic diversity and evolutionary rate of a region are shaped by a combination of evolutionary forces at different timescales (Hartl and Clark 2007). To understand why neighboring fragments in the 3D space show similar levels of diversity and divergence, we investigated the roles of different evolutionary forces that shape the polymorphism and evolutionary rates of large DNA fragments. We first assessed the contribution of the local

mutation rate, which varies in the eukaryotic genome at different scales (Hodgkinson and Eyre-Walker 2011; Terekhanova et al. 2017; Smith et al. 2018). We used the average substitution rate of putatively neutral sites (4-fold degenerate sites and NNSs) between *A. thaliana* and *A. lyrata* as a surrogate of the mutation rate and used the CCS simulation to assess the significance of the similarity between 3D neighboring fragments. The result shows that the observed difference is significantly smaller than that in the simulated networks (P-value < 0.001; fig. 3A), which suggests that the local mutation rate covaries between 3D adjacent fragments and plays a role in the correlated evolution between 3D neighbors. The conclusion is unaffected when we assess the similarity in mutation rate between 3D adjacent fragments using the divergence at 4-fold degenerate sites or NNSs alone as a proxy of the local mutation rate (P-value < 0.001 for both cases; supplementary fig. S6).

Evolutionary forces that contribute to the correlated evolution between 3D chromatin neighbors: purifying selection

To assess the contribution of selective constraints to the correlated evolution of neighboring fragments, we calculated various population genetic parameters to measure the strength and efficacy of purifying selection acting on a whole fragment or functional elements in the fragment. First, the level of excess rare variants can be interpreted as the relative strength of purifying selection across different classes of genomic regions (Altshuler et al. 2012; Khurana et al. 2013). Therefore, we calculated the fraction of rare SNPs with a derived allele frequency of less than 0.5% in each bin using polymorphism data from the 1001 Genomes Project (Alonso-Blanco et al. 2016). The result shows that the simulated networks using the CCS model present a higher degree of difference between nodes than the true network (P-value < 0.001; fig. 3B).

Next, we used the ratios of divergence and diversity of 0-fold versus 4-fold degenerate sites (denoted as d_0/d_4 and π_0/π_4, respectively) to quantify the strength or the efficacy of the negative selection acting on protein-coding genes in each fragment. For both d_0/d_4 and π_0/π_4, the average difference between connected nodes in the real network is significantly smaller than that in the simulated networks (P-value < 0.001 and P-value = 0.002 for d_0/d_4 and π_0/π_4, respectively; fig. 3C, D). Our results suggest that adjacent fragments and the genes they contain in the CIN are subjected to more similar evolutionary constraints than random pairs, which agrees with previous reports that neighboring genes in the 3D space present more similar functions and expression patterns than random gene pairs. We also compared the similarity of the strength and efficacy of the negative selection of potentially functional noncoding sequences (i.e., CNS+UTR) between chromatin neighbors to that of the null model. In these cases, we used putatively neutral noncoding sites (i.e., NNSs) as neutral comparators. The results show that the difference in $d_{CNS+UTR}/d_{NNS}$ between fragments in contact in the real network is marginally smaller than that in the simulated networks (P-value = 0.054; fig. 3E), while the disparity between the true data and the null model is significant for $\pi_{CNS+UTR}/\pi_{NNS}$ (P-value = 0.004; fig. 3F).

Evolutionary forces that contribute to the correlated evolution between 3D chromatin neighbors: positive selection

Although several studies have shown that the *A. thaliana* genome exhibits little evidence of genome-wide adaptive selection (Bustamante et al. 2002; Foxe et al. 2008; Wright and Andolfatto 2008; Gossmann et al. 2010; Slotte et al. 2011), substantial heterogeneity in the rate of positive selection across different categories of genes is also evident (Slotte et al. 2011). Do clusters of genes that are close to each other in the 3D space possess similar rates of adaptive

evolution? To answer this question, we calculated the proportion of adaptively driven substitutions (α) and the rate of adaptive substitution relative to the rate of neutral evolution (ω_a) for 0-fold sites in each 100 kb fragment using the software DFE-alpha (Eyre-Walker and Keightley 2009). We quantified these two measurements using divergence information from the *A. thaliana*-*A. lyrata* alignment and SNPs from two different populations, one containing 22 relict individuals from the Iberian Peninsula and the other comprising 50 accessions from Spain. For the results derived from the polymorphisms of the relict population, the average α at 0-fold sites in a 100 kb window is 20.27% (fig. 4A), which is substantially higher than the proportion previously reported, whereas the average α estimated using SNPs in the Spanish population is 6.24% (fig. 4D), a number that is very close to the results of previous studies (Gossmann et al. 2010; Slotte et al. 2011). The discrepancy in adaptive rates estimated using polymorphisms from the two populations could exist because the relict and Spanish populations have different historical effective population sizes. In the Spanish population, natural selection is less effective in removing slightly deleterious mutations and fixing slightly advantageous mutations because of the stronger effect of genetic drift in small populations, resulting in a reduction in α. When we compare the observed difference in α between neighboring nodes to that in the null model, no significant difference is found between the actual and simulated values for results derived from both the relict and Spanish populations (P-value = 0.923 and 0.639, respectively; fig. 4B, E). On the other hand, the difference in ω_a between neighboring fragments is significantly smaller than that in the simulated networks for estimates derived from both the relict and Spanish populations (P-value = 0.010 and 0.002, respectively; fig. 4C, F).

Genomic and epigenomic determinants of nucleotide diversity and divergence across the genome

Mutation, natural selection, and random genetic drift together shape the variation of genetic diversity within populations and divergence between species. Factors that affect these population genetic parameters thus may contribute to the observed correlated evolution between 3D neighbors. Such factors include recombination rates, GC content, gene density, replication timing, and chromatin organization (Makova and Hardison 2015). To elucidate the influence of various genetic and epigenetic features on the regional variation in genetic diversity and divergence and relate them to the large-scale correlated evolution in the 3D genome, we compiled a comprehensive set of genetic and epigenetic features that have been mapped genome wide in Arabidopsis (supplementary table S2). We first clustered these features using their pairwise correlation coefficients as a distance metric and found that they are largely clustered into two groups. The first group includes features associated with open chromatin, active transcription, and early replication timing, and the second group contains features associated with heterochromatin, inactive transcription, and late replication timing (fig. 5A). Remarkably, most epigenomic features associated with open chromatin present a strong anti-correlation with polymorphism and evolutionary rates (fig. 5B), with H3K36me3 shows the highest negative correlation with the substitution rate ($r = -0.74$, $P < 2.2 \times 10^{-16}$), while the density of DNase I hypersensitive sites (DHSs) in flowers exhibits the highest negative correlation with nucleotide diversity ($r = -0.60$, $P < 2.2 \times 10^{-16}$). On the other hand, histone variants and epigenetic marks that define heterochromatin and inactive transcription show an opposite trend, among which the histone variant H2A.W presents the highest positive correlation with the divergence between *A.*

thaliana and *A. lyrata* ($r = 0.69$, $P < 2.2 \times 10^{-16}$), while H3.1 presents the highest positive correlation with nucleotide diversity ($r = 0.64$, $P < 2.2 \times 10^{-16}$).

Chromatin organization has a great impact on the local mutation rate in the genome (Schuster-Bockler and Lehner 2012; Makova and Hardison 2015). Thus, the observed pattern of correlation between epigenetic marks and evolutionary parameters may be mediated by the influence of chromatin architecture on the local mutation rate. Indeed, we found that epigenetic features show the same trend of correlations with substitution rates at putatively neutral sites between *A. thaliana* and *A. lyrata* (which serves as a proxy of the mutation rate) as observed between epigenetic marks and nucleotide diversity and divergence, but to a lesser extent (fig. 5B). Using %(DAF<0.005) as a measure of selective constraint, we found that regions with higher levels of heterochromatin signals are subjected to lower selective constraints, and an opposite trend was observed for regions marked by higher levels of open chromatin signals. Taken together, these results support the notion that chromatin organization has a great influence on the evolution of regional DNA fragments, which is consistent with previous studies in humans (Schuster-Bockler and Lehner 2012; Makova and Hardison 2015).

Next, we sought to determine which genetic or epigenetic features have the most significant impact on regional nucleotide diversity and evolutionary rates and how much of the local variation in diversity and divergence can be explained by the combination of features. We applied a multiple regression model using increasing numbers of features to quantify the proportion of the variance of an evolutionary parameter that can be accounted for by the combination of features. We found that 57%, 70%, 64%, and 44% of the variance in nucleotide diversity, evolutionary rates, mutation rates, and selective constraint can be explained by combining all features (supplementary fig. S7). For polymorphisms within species, the histone

variant H3.1, which is enriched in silent regions of the genome (Stroud et al. 2012), accounts for 41% of the variance in regional genetic diversity and 28% of the variance in selective constraints. A considerable proportion of the variance in the divergence between species along the genome can be explained by a feature associated with transcription, H3K36me3 (Mahrez et al. 2016), where the explained proportion reaches 55% for overall divergence and 52% for divergence at putatively neutral sites. In contrast, the variance of the efficacy of natural selection is poorly explained by these features; only 18% and 7% of the variance in π_0/π_4 and ω_a can be explained by the combination of features, with no single feature explaining more than 5% of the variance in both cases.

To discern the evolutionary force through which the investigated genetic and epigenetic characteristics affect the observed correlated evolution, we carried out a partial least squares path modeling (PLS-PM) analysis. PLS-PM is a statistical method for analyzing complex multivariate relationships among variables, in which several observed variables are summarized into many fewer latent variables, and the path coefficients and their significances are calculated using a predefined causal network (Sanchez 2013). We used two latent variables to represent the two groups of features: group I contained features that are negatively correlated with genetic diversity and evolutionary rate, and group II included features that show positive correlations. The result of PLS-PM analysis shows that both groups have significant impacts on local mutation rates, but in opposite directions (path coefficient = -0.51 and 0.22 for group I and group II, respectively; fig. 5C). The mutation rate in turn significantly affects the evolutionary rate (path coefficient = 0.72), as expected from the neutral theory (Kimura 1983). However, mutation has little influence on genetic diversity. Only group II has a significant influence on the selective constraint, which in turn significantly affects diversity to a great extent and has a limited yet

significant influence on divergence. Neither group I nor group II has a significant impact on the efficacy of selection (measured as π_0/π_4). In addition, the two groups have direct influences on diversity and divergence, indicating that some of the variance in polymorphisms and evolutionary rates cannot be explained by our measures of mutation, selective constraint, and the efficacy of selection. The loadings and cross-loadings of the observed indicators with the two latent variables are shown in supplementary fig. S8.

Genomic features that have a greater influence on the genetic diversity and evolutionary rate of individual fragments also exhibit higher levels of assortativity in the CIN

Genetic and epigenetic features that have a significant influence on the variation in regional nucleotide diversity and evolutionary rates may not necessarily contribute to the correlated evolution of neighboring nodes in the CIN. To further explore which features make greater contributions to the correlated evolution between 3D neighboring fragments, we calculated the assortativity of each feature in the network. Assortativity measures the extent to which interacting nodes in a network present similar values for a feature, which is an approach that was first introduced in the social sciences (Newman 2002) and has been applied in CINs recently (Pancaldi et al. 2016). A higher positive assortativity of a feature means a higher propensity for neighboring nodes to present similar values. If a feature exhibits high assortativity in the network and has a significant influence on the regional variation of evolutionary rates, then this feature will make an important contribution to the correlated evolution between neighboring fragments in the 3D genome. Among the 39 genetic and epigenetic features, the occupancy of Pol II (assortativity = 0.211) and its variants (PolIISer2P, 0.269; PolIISer5P, 0.236), H3.1 (0.362), H2A.W (0.257) and H3K36ac (0.253) show relatively high levels of assortativity, whereas the

assortativity is very low for the density of replication origins (0.003) and recombination rates (0.010).

We further correlated the levels of the assortativity of features with their Pearson correlations with evolutionary parameters. Interestingly, those features exerting a greater influence on genetic diversity and evolutionary rates also present higher levels of assortativity (fig. 6A). For those features in group I, the correlations between the levels of assortativity and their correlations with diversity and divergence are 0.84 ($P = 2.9 \times 10^{-4}$) and 0.68 ($P = 1.0 \times 10^{-2}$), respectively, while the correlations for the features in group II are -0.86 ($P = 1.3 \times 10^{-8}$) and -0.79 ($P = 1.7 \times 10^{-6}$), respectively. Features with higher levels of assortativity also have a greater influence on local mutation rates and selective constraints (fig. 6B). The correlation between the levels of the assortativity of features and their effects on the evolution of local fragments is strong and significant, which may have profound implications for the organization of the eukaryotic genome. If a genetic or epigenetic feature that has a significant impact on the evolution of regional fragments but presents a very low level of assortativity, then the rapid evolution of one fragment may impose pressure on the evolution of its interacting counterpart, leading to functional incompatibility between the products of pairs of DNA fragments that are in contact.

Correlated evolution of large DNA fragments at the 50 kb scale

To confirm that our conclusions are not restricted to the scale (100 kb) that we presented in the previous sections, we repeated most of the main analyses at a 50 kb resolution, except for the assessment of the adaptive rate because there are too few genes in a window to obtain reliable estimates for this parameter. All the results are quantitatively similar to the results at a 100 kb

resolution (supplementary fig. S9-13), suggesting that the correlated evolution and its evolutionary and (epi)genomic determinants are general patterns at large scales in the Arabidopsis genome.

Discussion

Correlated evolution between biological units at various scales, whether derived from shared selective constraints or reciprocal evolutionary changes, has provoked the interests of biologists for a long time (Carmona et al. 2015). Here, we investigated the coordinated evolution of large DNA fragments based on the three-dimensional CINs in *A. thaliana* and examined the evolutionary forces and (epi)genomic features that potentially affect large-scale correlated evolution in the 3D genome. We found that both the genetic diversity and evolutionary rate are more similar between 3D chromatin neighbors than between random pairs, and that both mutation and selection play essential roles in the correlated evolution between neighboring DNA fragments. Chromatin organization has a major impact on regional genetic diversity and evolutionary rates in the genome. In addition, those (epi)genomic features that have a more significant influence on the evolution of local fragments also present higher levels of assortativity in the CIN, hence contributing more to the observed correlated evolution. The coordinated evolution of large-scale fragments in the genome inferred from our results will provide us new insights into the evolution and chromatin organization of the Arabidopsis genome and the organization of the eukaryotic genome in general.

It is well known that the organization of genes within eukaryotic genomes is not random at the one-dimensional scale (Hurst et al. 2004; Kosak and Groudine 2004); linked genes often

show comparable expression (Boutanaev et al. 2002; Williams and Bowles 2004) and evolve at similar rates (Williams and Hurst 2000). At the three-dimensional level, genes that are located close to each other present similar expression levels and protein functions (Ben-Elazar et al. 2013; Homouz and Kudlicki 2013; Diament et al. 2014). The present study extends our understanding of the organization of the eukaryotic genome by showing that adjacent large fragments carrying clusters of genes and other elements in the 3D genome evolve in a coordinated way. In addition, we focused on not only protein-coding genes and functional noncoding sequences but also on putatively non-functional sites, whose correlated evolution in the CIN has been shaped by evolutionary forces other than natural selection that directly act on them.

The observed covariation of genetic diversity and evolutionary rates between 3D neighboring fragments may be explained by the evolutionary forces that act on them. First, shared evolutionary pressure exerted on interacting functional elements such as protein-coding sequences and noncoding regulatory elements may contribute to the observed correlated evolution. This similarity of selective constraints could in turn be derived from comparable expression levels and breadths due to similar regulatory mechanisms acting on them (Babaei et al. 2015). Second, the proteins encoded by DNA sequences residing in neighboring fragments may interact with each other directly and coadapt, resulting in a coordinated evolutionary rate. Using adjusted mutual information as a measure of the correlated mutation between SNPs in Arabidopsis, Perlaza-Jimenez and Walther (2018) demonstrated that sites in physical contact at the 3D scale significantly overlap with pairs of genomic regions that are rich in correlated mutations, suggesting a potential role for compensatory mutations between 3D chromatin neighbors. Compensatory mutation does not exclusively occur between protein residues but can

also occur between noncoding sequences (Landry et al. 2005; Takahasi et al. 2011; Barriere et al. 2012) and between coding and regulatory sequences (Hershberg and Margalit 2006). In our simulation analyses, the difference in α between the protein-coding genes residing in 3D neighboring fragments is not significantly smaller than that in the random networks, but the difference in ω_a is significantly smaller than expected. Both α and ω_a are measures of adaptive evolution; $\alpha = \frac{D_{adaptive}}{D_{adaptive} + D_{nonadaptive}}$, and $\omega_a = \frac{D_{adaptive}}{D_{neutral}}$, where $D_{adaptive}$, $D_{nonadaptive}$, and $D_{neutral}$ are the rates of adaptive, nonadaptive, and neutral substitions, respectively. α measures the prevalence of adaptive evolution, while ω_a reflects the strength or efficacy of positive selection. For the purpose of comparison between species or genomic regions, ω_a is thought to be a more appropriate metric of adaptive evolution (Gossmann et al. 2012). Thus, in terms of the strength and efficacy of positive selection, our results suggest that genes residing in neighboring fragments at the 3D scale present more similar levels of adaptive evolution than expected.

For neutrally evolving sites, the genetic diversity is proportional to the effective population size and mutation rate ($\pi = 4N_e\mu$), while the evolutionary rate is equal to the mutation rate ($k = \mu$) (Kimura 1983). At both timescales, if a large fraction of nucleotides in a sequence are subjected to no or very weak selection, which is probably the case for the Hi-C fragments because their long consecutive sequences contain a significant proportion of noncoding DNA, then the mutation rate may play a dominant role in determining the similarity of genetic diversity and substitution rates. Indeed, our PLS-PM analysis showed that mutation has a significant impact on the evolutionary rates of large-scale fragments, but its influence on genetic diversity is limited. On the other hand, the mutation rate itself varies both within and across genomes (Baer et al. 2007; Hodgkinson and Eyre-Walker 2011) and is affected by various genomic and epigenomic features, among which the chromatin architecture is one of the decisive factors

(Schuster-Bockler and Lehner 2012; Makova and Hardison 2015). Consistent with previous studies in humans, we found that the mutation rate is elevated in genomic regions of closed chromatin and is suppressed in regions of open chromatin. The reduced mutation rate in regions with active gene expression may be attributed to transcription-coupled repair (Green et al. 2003), which is an additional repair mechanism that corrects errors in DNA before the next round of replication. Replication timing is another important determinant of mutation rate variation. Our results showed that mutation is reduced in regions with early replication and is enhanced in regions with late replication, corroborating the conclusion of previous studies (Makova and Hardison 2015). Furthermore, the combination of 39 (epi)genomic features can explain more than 60% of the variance of mutation rates across the genome at the 100 kb scale. In humans, more than 55% of the variance of somatic mutation rates can be explained by a combination of (epi)genomic features, whereas this proportion is reduced to 35% for germline mutation rate variation (Schuster-Bockler and Lehner 2012). The higher proportion of variance that can be explained by the (epi)genomic features in Arabidopsis compared to humans may stem from the fact that in plants, the soma and germen are not separated; therefore, the epigenomic features captured in somatic cells reflect the chromatin organization in germline cells to a greater extent in plant than in human cells.

Intriguingly, those genomic and epigenomic features that have a greater influence on regional mutation rates also present higher levels of assortativity in the network. In particular, many features associated with active transcription (e.g., Pol II and its phosphorylated forms, H3K36me3, and H3K36ac) exhibit both highly negative correlations with mutation rates and high levels of assortativity in the network. The histone variants that are associated with heterochromatin (H3.1 and H2A.W) (Yelagandula et al. 2014) also exhibit very high levels of

assortativity but highly positive correlations with the mutation rate. However, the assortativity of replication timing is moderate (0.179 and 0.145 for early and late replication, respectively), suggesting that the role of replication in the observed correlated mutation rates is not as significant as that of transcription. Overall, our findings suggest that chromatin organization affects not only the structure of the 3D genome but also the correlated evolution between neighboring fragments in the CIN.

In addition to natural selection and mutation rates, random genetic drift is a pivotal determinant of genetic diversity (Ellegren and Galtier 2016). When the effective population size is small, genetic drift will play a principal role in determining the fate of a newly arisen mutations, rather than natural selection, thus reducing the efficiency of natural selection. Similar to other evolutionary parameters, the effective population size is not constant across the genome (Charlesworth 2009). The within-genome variation of N_e is results from the differences in the strength of selection at linked sites (Charlesworth 2009), which is in turn associated with the local recombination rate and the density of selected sites (Cutter and Payseur 2013). Our simulation results showed that adjacent fragments do not present a similar rate of recombination (P-value = 0.911; supplementary fig. S14A) but exhibit comparable gene density (P-value < 0.001; supplementary fig. S14B), suggesting that the density of selected sites plays a more prominent role in reducing the disparities in N_e between neighboring fragments in the 3D genome. Although we did not explicitly test whether 3D neighbors in the chromatin network possessed more similar N_e due to the complexity of explicitly estimating this parameter, the analyses of the efficacy of negative and positive selection (measured as π_0/π_4 and ω_a, respectively) indicated that genomic regions that are located close to each other in the 3D space

present similar N_e, which do not generate considerable discrepancy in the efficacy of natural selection between fragment pairs in contact with each other.

In the present study, we investigated the large-scale coordinated evolution in only one species, the model plant *A. thaliana*. The genome of this species has some properties that differ from those of other eukaryotic organisms. First, the genome of *A. thaliana* is small and compact (~125 Mb), and the density of coding sequences is relatively high compared to that in other species possessing a large genome. Second, as a predominantly selfing species, the effective recombination rate is rather low in *A. thaliana*. These two properties together affect linked selection in the genome, which in turn affects genetic diversity (Ellegren and Galtier 2016). Third, some characteristics of chromatin organization in the nucleus of *A. thaliana* differ from those in other species. For example, the topologically associated domain (TAD) is a conspicuous characteristic of the chromatin architecture in mammals and has also recently been found in rice (*Oryza sativa*) (Liu et al. 2017), whereas this structure is not prominent in *A. thaliana* (Dogan and Liu 2018). A preliminary analysis in rice suggests that genome size and the density of coding sequences do not affect the correlated evolution between large DNA fragments in the CIN (supplementary fig. S15). However, whether the observed pattern of coordinated evolution can be extrapolated to other species requires further investigation.

Materials and Methods

Construction of the CINs

The raw reads from two Hi-C datasets from *A. thaliana* (Wang et al. 2015; Liu et al. 2016) were downloaded from the NCBI Sequence Read Archive. Since these two datasets represent the

average chromatin architecture in the same tissue of Arabidopsis at the same developmental stage (i.e., the aerial portions of 10-day-old seedlings), we combined the short reads from these two studies to detect chromatin interactions, as did Liu et al. (2016). The reads were mapped to the *A. thaliana* genome (TAIR10) using bowtie2 (Langmead and Salzberg 2012) with default parameters, and PCR duplicates and reads mapped to multiple locations in the genome were removed from downstream analysis. We applied two different strategies to detect significant intra- and inter-chromosomal contacts. For intra-chromosomal interactions, we used Fit-Hi-C (Ay, Bailey, et al. 2014) to identify high-confidence contacts with the default parameters. We used an FDR cutoff of 0.05 to remove low-confidence intra-chromosomal contacts. For contacts between chromosomes, it is difficult to model the null distribution of contacts since there is no trend of decreasing interaction probability with increasing linear distance. Thus, we applied a uniform probability model to calculate the P-values of interactions as described previously (Duan et al. 2010; Xie et al. 2016). We carried out multiple test corrections and applied a stringent FDR cutoff of 0.0001 to remove the noise of the Hi-C data. The CIN was constructed with both intra- and inter-chromosomal high-confidence contacts using the igraph package (version 1.2.4) (Csardi and Nepusz 2006) in R.

Because the DFE-alpha method is not suitable for estimating the rate of adaptive evolution with a small number of genes (see the "Inference of natural selection" section), we removed individual 100 kb fragments with no more than 15 protein-coding genes from the chromatin network construction procedure and all downstream analyses. Furthermore, we removed fragments for which more than 80% of nucleotides could not be aligned to *A. lyrata* or masked as repeat sequences in either the *A. thaliana* genome or their corresponding aligned sequences in *A. lyrata*.

To test our hypothesis at different scales, we also constructed a CIN at a 50 kb resolution using the same Hi-C data and methods as indicated above, but we removed individual windows with less than eight genes and more than 80% of unmappable sites. A CIN with a 100 kb resolution was constructed for rice using data from Liu et al. (2017), in which fragments with less than eight genes and more than 80% unmappable sequences were discarded.

Calculation of genetic diversity and divergence

Polymorphism data for *A. thaliana* were downloaded from the 1001 Genomes website (http://1001genomes.org), which contains genome-wide SNPs and indels from 1,135 globally distributed Arabidopsis accessions (Alonso-Blanco et al. 2016). We filtered out SNPs with more than two alleles and insertion/deletion (indel) polymorphisms, resulting in 10,707,430 biallelic SNPs. The averaged nucleotide diversity (π) was calculated for each nonoverlapping 100 kb or 50 kb window to represent the genetic diversity of fragments. Additionally, the average π for 0-fold nonsynonymous sites, 4-fold synonymous sites, putatively functional noncoding sequences, and putatively neutral noncoding sequences were calculated for each fragment. The putatively functional noncoding sequences were defined as the conserved noncoding sequences (CNS) identified by Haudry et al. (2013) plus the untranslated regions (5'UTR and 3'UTR), abbreviated as CNS+UTR. The putatively neutral noncoding sequences (NNSs) were defined as the noncoding sequences excluding the CNS+UTR sequences and nucleotides that are identified as belonging to DHSs in PlantTFDB 4.0 (http://planttfdb.cbi.pku.edu.cn) (Jin et al. 2017). Nucleotide diversity for each 100 kb nonoverlapping window in rice was computed using biallelic SNPs in the Geng/Japonica population from the 3,000 Rice Genomes Project (Wang et al. 2018).

Regarding the evolutionary rates of fragments, we calculated the divergence between *A. thaliana* and *A. lyrata* for each fragment, as well as the divergence at sites with different functional constraints in each window. Whole-genome alignment between *A. thaliana* and *A. lyrata* was carried out using LASTZ (Harris 2007), followed by chaining and netting (Kent et al. 2003). Blocks shorter than 100 bp were discarded. Any site that was masked as part of a repeat sequence in either *A. thaliana* or *A. lyrata* was excluded from the divergence analysis. We used the Nei-Gojobori method (Nei and Gojobori 1986) to calculate divergence between the two species. For rice, we aligned the *O. sativa* cv. Nipponbare IRGSP 1.0 reference genome to the *O. meridionalis* genome using LASTZ and calculated the overall divergence in each 100 kb window using the same method as in Arabidopsis.

Inference of natural selection

Several parameters were calculated to quantify the strength and efficiency of negative selection and positive selection for each fragment in the CIN. First, we quantified the strength of selective constraints as the proportion of SNPs with a derived allele frequency of less than 0.5% in the global collection of Arabidopsis in each window. Ancestral alleles were derived from whole-genome alignment with *A. lyrata*. Second, we calculated the ratio of 0-fold nonsynonymous versus 4-fold synonymous nucleotide diversity (π_0/π_4) and the ratio of nucleotide diversity at putatively functional noncoding sites to diversity at neutral noncoding positions ($\pi_{CNS+UTR}/\pi_{NNS}$) in each window as the strength or efficiency of purifying selection on protein-coding genes and functional noncoding sequences, respectively.

We also computed the fraction of adaptive nucleotide substitutions (α) and the rate of adaptive evolution relative to the rate of neutral evolution (ω_a) using the DFE-alpha approach (Eyre-Walker and Keightley 2009) for 0-fold degenerate sites. The DFE-alpha method simultaneously estimates the distribution of fitness effects (DFE) of new deleterious mutations and the rate of adaptive evolution, in which it accounts for the effects of demographic changes and slightly deleterious mutations on the estimation. Because DFE-alpha is inappropriate for estimating DFE and α using large samples (Kim et al. 2017), we restricted our analyses to the 22 accessions from the ancestral population on the Iberian Peninsula or 50 individuals from the more recent Spanish population. DFE was estimated under a 2-epoch model in which a stepwise population size change was applied. The Jukes-Cantor model was applied to correct the substitution rate between species, and polymorphic sites were removed when calculating α and ω_a.

Simulation (P-value computation)

We applied a conservative empirical null model, the cyclic chromosome shift model (Diament et al. 2014), to test whether fragments in direct contact in the CIN evolve in a coordinated way and whether chromatin organization plays a role in the coordinated evolution of 3D neighbors. Specifically, we preserved the spatial configuration of the Hi-C network and randomly shifted the location of Hi-C bins along their respective chromosomes. By doing so, the linear adjacency between fragments along the "circular" chromosomes remains unchanged, but the contact relationships between fragments in the 3D structure are perturbed. We generated 1,000 simulated networks and calculated the P-value as the number of networks in which the mean value of the difference of a parameter between neighboring nodes is smaller than that in the actual spatial conformation. We also employed other empirical null models: degree-preserving rewiring of the

network and cyclic genome shift, in which fragments are allowed to rotate and move between different chromosomes.

Genome-wide feature data processing and regression analysis

Short reads for DHSs, histone acetylations, histone methylations, the occupancy of histones and Pol II and their variants were downloaded from NCBI (see supplementary table S2 for a complete list of source references and SRA accession numbers), then mapped to the Arabidopsis reference genome (TAIR10), and PCR duplicates were filtered out. The relative density of a feature in a 100 kb window was calculated as the log2-transformed and normalized read count with a mean of 0 and a standard deviation of 1. Gene density was calculated as the total number of nucleotides covered by genes (including introns) in a window divided by the length of the window. Gene-level recombination rates were retrieved from Marais et al. (2004) and averaged for each 100 kb or 50 kb window. The GC content was computed as the fraction of G and C nucleotides in a window. The annotation of transposable elements (TEs) in *A. thaliana* was downloaded from The Arabidopsis Information Resource (TAIR) website (www.arabidopsis.org), and CpG islands in the Arabidopsis genome were identified using CpGIScan (Jian et al. 2017). The coverage of TEs and CpG islands was calculated as the fractions of nonoverlapping TEs and CpG islands in a window, respectively. Gene order conservation scores were retrieved from the Ensembl Plants database (http://plants.ensembl.org) and averaged for each window. The coverage of replication origins was calculated using data from Vergara et al. (2017). The replication timing of three categories (i.e., early, mid, and late) was computed using data from Concia et al. (2018).

To determine which genomic features correlate with and contribute to the variation of genetic diversity and evolutionary rates in the Arabidopsis genome, we first calculated the Pearson's correlation coefficients of each evolutionary parameter with the above 39 genomic features using the "cor.test" function in R. We then performed multiple linear regression analyses using the genomic features as independent variables and each focal evolutionary parameter as a dependent variable with forward stepwise selection using the "regsubsets" function of the leaps R package. A PLS-PM analysis was carried out to infer the underlying relationships among (epi)genomic features, evolutionary forces, genetic diversity, and evolutionary rates using the R package plspm (Sanchez 2013). We used two latent variables (group I and group II) to represent the 39 genomic and epigenomic features; group I summarizes the features that present negative correlations with genetic diversity and evolutionary rates, and group II represents the features that are positively correlated with diversity and divergence.

Network analysis

We calculated the assortativity of each of the 39 genomic features in the CIN using the "assortativity" function of the igraph R package. For continuous variables, assortativity is defined as

$$r = \frac{1}{\sigma_q^2} \sum_{jk} jk(e_{jk} - q_j q_k)$$

where $q_i = \sum_j e_{ij}$, e_{ij} is the fraction of edges connecting vertices of type i and j, and σ_q is the standard deviation of q (Newman 2002). If the assortativity of a feature is high, it means that connected nodes tend to exhibit similar values.

Supplementary Material

Supplementary tables S1-S2 and figures S1-S15 are attached separately.

Acknowledgments

The authors thank Bing Su, Kai Zeng, and Tian Tang for valuable discussions regarding this work. This work was supported by the Fundamental Research Funds for the Central Universities (Z109021804) to Y.Y. and the National Natural Science Foundation of China (31670321), the Hundred Talents Program of Shaanxi Province of China (A289021612), and the Fund of Northwest A&F University (Z111021404) to R.Y.

Author Contributions

R.Y. conceived and designed the research; Y.Y. and Z.L. collected and analyzed the data with input from all authors; Y.Y. wrote the manuscript with input from R.Y. and Z.L.

References

Alonso-Blanco C, Andrade J, Becker C, Bemm F, Bergelson J, Borgwardt KM, Cao J, Chae E, Dezwaan TM, Ding W, et al. 2016. 1,135 genomes reveal the global pattern of polymorphism in *Arabidopsis thaliana*. *Cell*. 166:481-491.

Altshuler DM, Durbin RM, Abecasis GR, Bentley DR, Chakravarti A, Clark AG, Donnelly P, Eichler EE, Flicek P, Gabriel SB, et al. 2012. An integrated map of genetic variation from 1,092 human genomes. *Nature*. 491:56-65.

Alvarez-Ponce D, Fares MA. 2012. Evolutionary rate and duplicability in the *Arabidopsis thaliana* protein-protein interaction network. *Genome Biol Evol*. 4:1263-1274.

Ay F, Bailey TL, Noble WS. 2014. Statistical confidence estimation for Hi-C data reveals regulatory chromatin contacts. *Genome Res*. 24:999-1011.

Ay F, Bunnik EM, Varoquaux N, Bol SM, Prudhomme J, Vert JP, Noble WS, Le Roch KG. 2014. Three-dimensional modeling of the *P. falciparum* genome during the erythrocytic cycle reveals a strong connection between genome architecture and gene expression. *Genome Res*. 24:974-988.

Babaei S, Mahfouz A, Hulsman M, Lelieveldt BP, de Ridder J, Reinders M. 2015. Hi-C chromatin interaction networks predict co-expression in the mouse cortex. *Plos Comput Biol*. 11:e1004221.

Baer CF, Miyamoto MM, Denver DR. 2007. Mutation rate variation in multicellular eukaryotes: causes and consequences. *Nat Rev Genet*. 8:619-631.

Barreto FS, Burton RS. 2013. Evidence for compensatory evolution of ribosomal proteins in response to rapid divergence of mitochondrial rRNA. *Mol Biol Evol*. 30:310-314.

Barreto FS, Watson ET, Lima TG, Willett CS, Edmands S, Li W, Burton RS. 2018. Genomic signatures of mitonuclear coevolution across populations of *Tigriopus californicus*. *Nat Ecol Evol*.

Barriere A, Gordon KL, Ruvinsky I. 2012. Coevolution within and between regulatory loci can preserve promoter function despite evolutionary rate acceleration. *Plos Genet*. 8:e1002961.

Ben-Elazar S, Yakhini Z, Yanai I. 2013. Spatial localization of co-regulated genes exceeds genomic gene clustering in the *Saccharomyces cerevisiae* genome. *Nucleic Acids Res*. 41:2191-2201.

Bonev B, Cavalli G. 2016. Organization and function of the 3D genome. *Nat Rev Genet*. 17:661-678.

Boutanaev AM, Kalmykova AI, Shevelyov YY, Nurminsky DI. 2002. Large clusters of co-expressed genes in the Drosophila genome. *Nature*. 420:666-669.

Burdon JJ, Thrall PH. 2009. Coevolution of plants and their pathogens in natural habitats. *Science*. 324:755-756.

Bustamante CD, Nielsen R, Sawyer SA, Olsen KM, Purugganan MD, Hartl DL. 2002. The cost of inbreeding in Arabidopsis. *Nature*. 416:531-534.

Carmona D, Fitzpatrick CR, Johnson MT. 2015. Fifty years of co-evolution and beyond: integrating co-evolution from molecules to species. *Mol Ecol*. 24:5315-5329.

Charlesworth B. 2009. Fundamental concepts in genetics: effective population size and patterns of molecular evolution and variation. *Nat Rev Genet*. 10:195-205.

Concia L, Brooks AM, Wheeler E, Zynda GJ, Wear EE, LeBlanc C, Song J, Lee TJ, Pascuzzi PE, Martienssen RA, et al. 2018. Genome-wide analysis of the Arabidopsis replication timing program. *Plant Physiol*. 176:2166-2185.

Csardi G, Nepusz T. 2006. The igraph software package for complex network research. *InterJournal Complex Sys*. 1695:1695.

Cutter AD, Payseur BA. 2013. Genomic signatures of selection at linked sites: unifying the disparity among species. *Nat Rev Genet*. 14:262-274.

de Juan D, Pazos F, Valencia A. 2013. Emerging methods in protein co-evolution. *Nat Rev Genet*. 14:249-261.

Diament A, Pinter RY, Tuller T. 2014. Three-dimensional eukaryotic genomic organization is strongly correlated with codon usage expression and function. *Nat Commun*. 5:5876.

Dogan ES, Liu C. 2018. Three-dimensional chromatin packing and positioning of plant genomes. *Nat Plants*. 4:521-529.

Duan Z, Andronescu M, Schutz K, McIlwain S, Kim YJ, Lee C, Shendure J, Fields S, Blau CA, Noble WS. 2010. A three-dimensional model of the yeast genome. *Nature*. 465:363-367.

Ehrlich PR, Raven PH. 1964. Butterflies and plants: a study in coevolution. *Evolution*. 18:586-608.

Ellegren H, Galtier N. 2016. Determinants of genetic diversity. *Nat Rev Genet*. 17:422-433.

Eyre-Walker A, Keightley PD. 2009. Estimating the rate of adaptive molecular evolution in the presence of slightly deleterious mutations and population size change. *Mol Biol Evol*. 26:2097-2108.

Feng S, Cokus SJ, Schubert V, Zhai J, Pellegrini M, Jacobsen SE. 2014. Genome-wide Hi-C analyses in wild-type and mutants reveal high-resolution chromatin interactions in Arabidopsis. *Mol Cell*. 55:694-707.

Foxe JP, Dar VU, Zheng H, Nordborg M, Gaut BS, Wright SI. 2008. Selection on amino acid substitutions in Arabidopsis. *Mol Biol Evol*. 25:1375-1383.

Fraser HB, Hirsh AE, Steinmetz LM, Scharfe C, Feldman MW. 2002. Evolutionary rate in the protein interaction network. *Science*. 296:750-752.

Gossmann TI, Keightley PD, Eyre-Walker A. 2012. The effect of variation in the effective population size on the rate of adaptive molecular evolution in eukaryotes. *Genome Biol Evol*. 4:658-667.

Gossmann TI, Song BH, Windsor AJ, Mitchell-Olds T, Dixon CJ, Kapralov MV, Filatov DA, Eyre-Walker A. 2010. Genome wide analyses reveal little evidence for adaptive evolution in many plant species. *Mol Biol Evol*. 27:1822-1832.

Gossmann TI, Woolfit M, Eyre-Walker A. 2011. Quantifying the variation in the effective population size within a genome. *Genetics*. 189:1389-1402.

Green P, Ewing B, Miller W, Thomas PJ, Program NCS, Green ED. 2003. Transcription-associated mutational asymmetry in mammalian evolution. *Nat Genet*. 33:514-517.

Harris RS. 2007. Improved pairwise alignment of genomic DNA. PhD thesis. Pennsylvania State University.

Hartl DL, Clark AG. 2007. Principles of population genetics. Sunderland: Sinauer Associates.

Haudry A, Platts AE, Vello E, Hoen DR, Leclercq M, Williamson RJ, Forczek E, Joly-Lopez Z, Steffen JG, Hazzouri KM, et al. 2013. An atlas of over 90,000 conserved noncoding sequences provides insight into crucifer regulatory regions. *Nat Genet*. 45:891-U228.

Hershberg R, Margalit H. 2006. Co-evolution of transcription factors and their targets depends on mode of regulation. *Genome Biol*. 7:R62.

Hodgkinson A, Eyre-Walker A. 2011. Variation in the mutation rate across mammalian genomes. *Nat Rev Genet*. 12:756-766.

Homouz D, Kudlicki AS. 2013. The 3D organization of the yeast genome correlates with co-expression and reflects functional relations between genes. *Plos One*. 8:e54699.

Hurst LD, Pal C, Lercher MJ. 2004. The evolutionary dynamics of eukaryotic gene order. *Nat Rev Genet*. 5:299-310.

Jian ZY, Du LM, Zhang XY, Yue BS, Fan ZX. 2017. CpGIScan: An ultrafast tool for CpG islands identification from genome sequence. *Curr Bioinform*. 12:181-184.

Jin J, Tian F, Yang DC, Meng YQ, Kong L, Luo J, Gao G. 2017. PlantTFDB 4.0: toward a central hub for transcription factors and regulatory interactions in plants. *Nucleic Acids Res*. 45:D1040-D1045.

Juan D, Pazos F, Valencia A. 2008. Co-evolution and co-adaptation in protein networks. *Febs Lett*. 582:1225-1230.

Kent WJ, Baertsch R, Hinrichs A, Miller W, Haussler D. 2003. Evolution's cauldron: Duplication, deletion, and rearrangement in the mouse and human genomes. *Proceedings of the National Academy of Sciences*. 100:11484.

Kern AD, Kondrashov FA. 2004. Mechanisms and convergence of compensatory evolution in mammalian mitochondrial tRNAs. *Nat Genet*. 36:1207-1212.

Khurana E, Fu Y, Colonna V, Mu XJ, Kang HM, Lappalainen T, Sboner A, Lochovsky L, Chen J, Harmanci A, et al. 2013. Integrative annotation of variants from 1092 humans: application to cancer genomics. *Science*. 342:1235587.

Kim BY, Huber CD, Lohmueller KE. 2017. Inference of the distribution of selection coefficients for new nonsynonymous mutations using large samples. *Genetics*. 206:345-361.

Kimura M. 1983. The neutral theory of molecular evolution. Cambridge: Cambridge University Press.

Kondrashov AS, Sunyaev S, Kondrashov FA. 2002. Dobzhansky-Muller incompatibilities in protein evolution. *P Natl Acad Sci USA*. 99:14878-14883.

Kosak ST, Groudine M. 2004. Gene order and dynamic domains. *Science*. 306:644-647.

Landry CR, Wittkopp PJ, Taubes CH, Ranz JM, Clark AG, Hartl DL. 2005. Compensatory cis-trans evolution and the dysregulation of gene expression in interspecific hybrids of Drosophila. *Genetics*. 171:1813-1822.

Langmead B, Salzberg SL. 2012. Fast gapped-read alignment with Bowtie 2. *Nat Methods*. 9:357-359.

Levin L, Blumberg A, Barshad G, Mishmar D. 2014. Mito-nuclear co-evolution: the positive and negative sides of functional ancient mutations. *Frontiers in Genetics*. 5.

Lieberman-Aiden E, van Berkum NL, Williams L, Imakaev M, Ragoczy T, Telling A, Amit I, Lajoie BR, Sabo PJ, Dorschner MO, et al. 2009. Comprehensive mapping of long-range interactions reveals folding principles of the human genome. *Science*. 326:289-293.

Liu C, Cheng Y-J, Wang J-W, Weigel D. 2017. Prominent topologically associated domains differentiate global chromatin packing in rice from Arabidopsis. *Nature Plants*. 3:742-748.

Liu C, Wang C, Wang G, Becker C, Zaidem M, Weigel D. 2016. Genome-wide analysis of chromatin packing in *Arabidopsis thaliana* at single-gene resolution. *Genome Res*. 26:1057-1068.

Mahrez W, Arellano MS, Moreno-Romero J, Nakamura M, Shu H, Nanni P, Kohler C, Gruissem W, Hennig L. 2016. H3K36ac is an evolutionary conserved plant histone modification that marks active genes. *Plant Physiol*. 170:1566-1577.

Makova KD, Hardison RC. 2015. The effects of chromatin organization on variation in mutation rates in the genome. *Nat Rev Genet*. 16:213-223.

Marais G, Charlesworth B, Wright SI. 2004. Recombination and base composition: the case of the highly self-fertilizing plant *Arabidopsis thaliana*. *Genome Biol*. 5:R45.

Nei M, Gojobori T. 1986. Simple methods for estimating the numbers of synonymous and nonsynonymous nucleotide substitutions. *Mol Biol Evol*. 3:418-426.

Newman MEJ. 2002. Assortative mixing in networks. *Phys Rev Lett*. 89: 208701.

Osada N, Akashi H. 2012. Mitochondrial-nuclear interactions and accelerated compensatory evolution: evidence from the primate cytochrome C oxidase complex. *Mol Biol Evol*. 29:337-346.

Pal C, Papp B, Lercher MJ. 2006. An integrated view of protein evolution. *Nat Rev Genet*. 7:337-348.

Pancaldi V, Carrillo-de-Santa-Pau E, Javierre BM, Juan D, Fraser P, Spivakov M, Valencia A, Rico D. 2016. Integrating epigenomic data and 3D genomic structure with a new measure of chromatin assortativity. *Genome Biol*. 17:152.

Parmakelis A, Kotsakiozi P, Rand D. 2013. Animal mitochondria, positive selection and cyto-nuclear coevolution: insights from pulmonates. *Plos One*. 8:e61970.

Pazos F, Valencia A. 2008. Protein co-evolution, co-adaptation and interactions. *Embo J*. 27:2648-2655.

Perlaza-Jimenez L, Walther D. 2018. A genome-wide scan for correlated mutations detects macromolecular and chromatin interactions in Arabidopsis thaliana. *Nucleic Acids Res*.

Rand DM, Haney RA, Fry AJ. 2004. Cytonuclear coevolution: the genomics of cooperation. *Trends Ecol Evol*. 19:645-653.

Ruiz-Velasco M, Zaugg JB. 2017. Structure meets function: How chromatin organisation conveys functionality. *Current Opinion in Systems Biology*. 1:129-136.

Sanchez G. 2013. PLS Path Modeling with R.

Schuster-Bockler B, Lehner B. 2012. Chromatin organization is a major influence on regional mutation rates in human cancer cells. *Nature*. 488:504-507.

Segurel L, Wyman MJ, Przeworski M. 2014. Determinants of mutation rate variation in the human germline. *Annu Rev Genomics Hum Genet*. 15:47-70.

Sloan DB, Warren JM, Williams AM, Wu Z, Abdel-Ghany SE, Chicco AJ, Havird JC. 2018. Cytonuclear integration and co-evolution. *Nat Rev Genet*.

Slotte T, Bataillon T, Hansen TT, St Onge K, Wright SI, Schierup MH. 2011. Genomic determinants of protein evolution and polymorphism in Arabidopsis. *Genome Biol Evol*. 3:1210-1219.

Smith TCA, Arndt PF, Eyre-Walker A. 2018. Large scale variation in the rate of germ-line de novo mutation, base composition, divergence and diversity in humans. *Plos Genet*. 14:e1007254.

Stamatoyannopoulos JA, Adzhubei I, Thurman RE, Kryukov GV, Mirkin SM, Sunyaev SR. 2009. Human mutation rate associated with DNA replication timing. *Nat Genet*. 41:393-395.

Stroud H, Otero S, Desvoyes B, Ramirez-Parra E, Jacobsen SE, Gutierrez C. 2012. Genome-wide analysis of histone H3.1 and H3.3 variants in *Arabidopsis thaliana*. *P Natl Acad Sci USA*. 109:5370-5375.

Takahasi KR, Matsuo T, Takano-Shimizu-Kouno T. 2011. Two types of cis-trans compensation in the evolution of transcriptional regulation. *P Natl Acad Sci USA*. 108:15276-15281.

Terekhanova NV, Seplyarskiy VB, Soldatov RA, Bazykin GA. 2017. Evolution of local mutation rate and its determinants. *Mol Biol Evol*. 34:1100–1109.

Vergara Z, Sequeira-Mendes J, Morata J, Peiro R, Henaff E, Costas C, Casacuberta JM, Gutierrez C. 2017. Retrotransposons are specified as DNA replication origins in the gene-poor regions of Arabidopsis heterochromatin. *Nucleic Acids Res*. 45:8358-8368.

Wang C, Liu C, Roqueiro D, Grimm D, Schwab R, Becker C, Lanz C, Weigel D. 2015. Genome-wide analysis of local chromatin packing in *Arabidopsis thaliana*. *Genome Res*. 25:246-256.

Wang W, Mauleon R, Hu Z, Chebotarov D, Tai S, Wu Z, Li M, Zheng T, Fuentes RR, Zhang F, et al. 2018. Genomic variation in 3,010 diverse accessions of Asian cultivated rice. *Nature*. 557:43-49

Weng ML, Ruhlman TA, Jansen RK. 2016. Plastid-nuclear interaction and accelerated coevolution in plastid ribosomal genes in Geraniaceae. *Genome Biol Evol*. 8:1824-1838.

Williams EJB, Bowles DJ. 2004. Coexpression of neighboring genes in the genome of *Arabidopsis thaliana*. *Genome Res*. 14:1060-1067.

Williams EJB, Hurst LD. 2000. The proteins of linked genes evolve at similar rates. *Nature*. 407:900-903.

Woo YH, Li WH. 2012. DNA replication timing and selection shape the landscape of nucleotide variation in cancer genomes. *Nat Commun*. 3.

Wright SI, Andolfatto P. 2008. The impact of natural selection on the genome: emerging patterns in Drosophila and Arabidopsis. *Annu Rev Ecol Syst*. 39:193-213.

Xie T, Yang QY, Wang XT, McLysaght A, Zhang HY. 2016. Spatial colocalization of human ohnolog pairs acts to maintain dosage-balance. *Mol Biol Evol*. 33:2368-2375.

Yelagandula R, Stroud H, Holec S, Zhou K, Feng S, Zhong X, Muthurajan UM, Nie X, Kawashima T, Groth M, et al. 2014. The histone variant H2A.W defines heterochromatin and promotes chromatin condensation in Arabidopsis. *Cell*. 158:98-109.

Zeng K, Jackson BC. 2018. Methods for estimating demography and detecting between-locus differences in the effective population size and mutation rate. *Mol Biol Evol*.

Zhang J, Ruhlman TA, Sabir J, Blazier JC, Jansen RK. 2015. Coordinated rates of evolution between interacting plastid and nuclear genes in Geraniaceae. *Plant Cell*. 27:563-573.

Zhang JZ, Yang JR. 2015. Determinants of the rate of protein sequence evolution. *Nat Rev Genet*. 16:409-420.

Figure Legends

Figure 1. Fragments with more connections in the CIN are subjected to higher levels of selective constraints and evolve more slowly. The four panels show the correlation between the degree in the CIN and nucleotide diversity (A), %(DAF<0.005) (B), evolutionary rates (C), and the number of genes (D). The gray line and shaded area are the loess fitting line and its 95% confidence interval, respectively.

Figure 2. Large DNA fragments that are in direct contact in the CIN display a similar genetic diversity and evolutionary rate, and this similarity cannot be explained by their linear adjacency. The upper two panels show the distribution of the mean difference in genetic diversity (A) and evolutionary rates (B) between adjacent fragments in 1,000 simulated networks using the CCS null model. The blue lines show the simulated distribution of a parameter, while the red arrow represents the observed mean difference of a parameter. The P-value calculated as the number of mean differences in simulated networks less than the observed difference is shown at the top left. The lower two panels show that the similarity in genetic diversity (C) and evolutionary rates (D) between fragment pairs decreases when the 3D distance between them increases. *** P-value < 0.001, NS: nonsignificant.

Figure 3. Neighboring fragments in the CIN exhibit similar regional mutation rates and evolutionary constraints. The observed average difference and the distribution of the average difference between adjacent nodes in simulated networks are shown for divergence at putatively neutral sites ($d_{Neutral}$; A), %(DAF<0.005) (B), d_0/d_4 (C), π_0/π_4 (D), $d_{CNS+UTR}/d_{NNS}$ (E), and $\pi_{CNS+UTR}/\pi_{NNS}$ (F).

Figure 4. Rate of adaptive evolution and similarity of positive selection between 3D neighboring fragments. The upper three panels show the distribution of α (A) in 100 kb fragments and the results of CCS simulations for α (B) and ω_a (C) using polymorphism data from the relict population. The lower three panels show the distribution of α (A) in 100 kb fragments and the results of CCS simulations for α (B) and ω_a (C) using polymorphism data from the Spanish population.

Figure 5. A set of diverse genomic and epigenomic features affect local nucleotide diversity and evolutionary rates along the genome. (A) Correlation heatmap of 39 genomic and epigenomic features. (B) Pearson's correlation coefficients of divergence, genetic diversity, divergence at putatively neutral sites and 1 - %(DAF<0.005) with diverse genomic and epigenomic features in 100 kb nonoverlapping windows. (C) The result of PLS-PM showing the causal relationship between the two groups of features and evolutionary parameters. Divergence at putatively neutral sites, %(DAF<0.005), and π_0/π_4 are used to represent mutations, selective constraint, and the efficacy of selection, respectively. Arrows represent the predefined causal directions between variables; red indicates a negative impact and blue a positive one. The path coefficients and their significance are labeled beside the arrows. *** P-value < 0.001, ** P-value < 0.01, and * P-value < 0.05.

Figure 6. Genomic and epigenomic features that have a higher impact on the evolution of regional sequences exhibit higher levels of assortativity in the CIN. The x-axis gives the Pearson's correlation coefficient of each genomic feature with a specific evolutionary parameter. (A) purple: genetic diversity, and blue: evolutionary rate; (B) purple: selective constraint, and blue: mutation rate. The y-axis gives the assortativity of each feature in the CIN. The solid lines represent the linear best fits that were obtained for Pearson's r > 0 and r < 0 separately.

Figure 1.

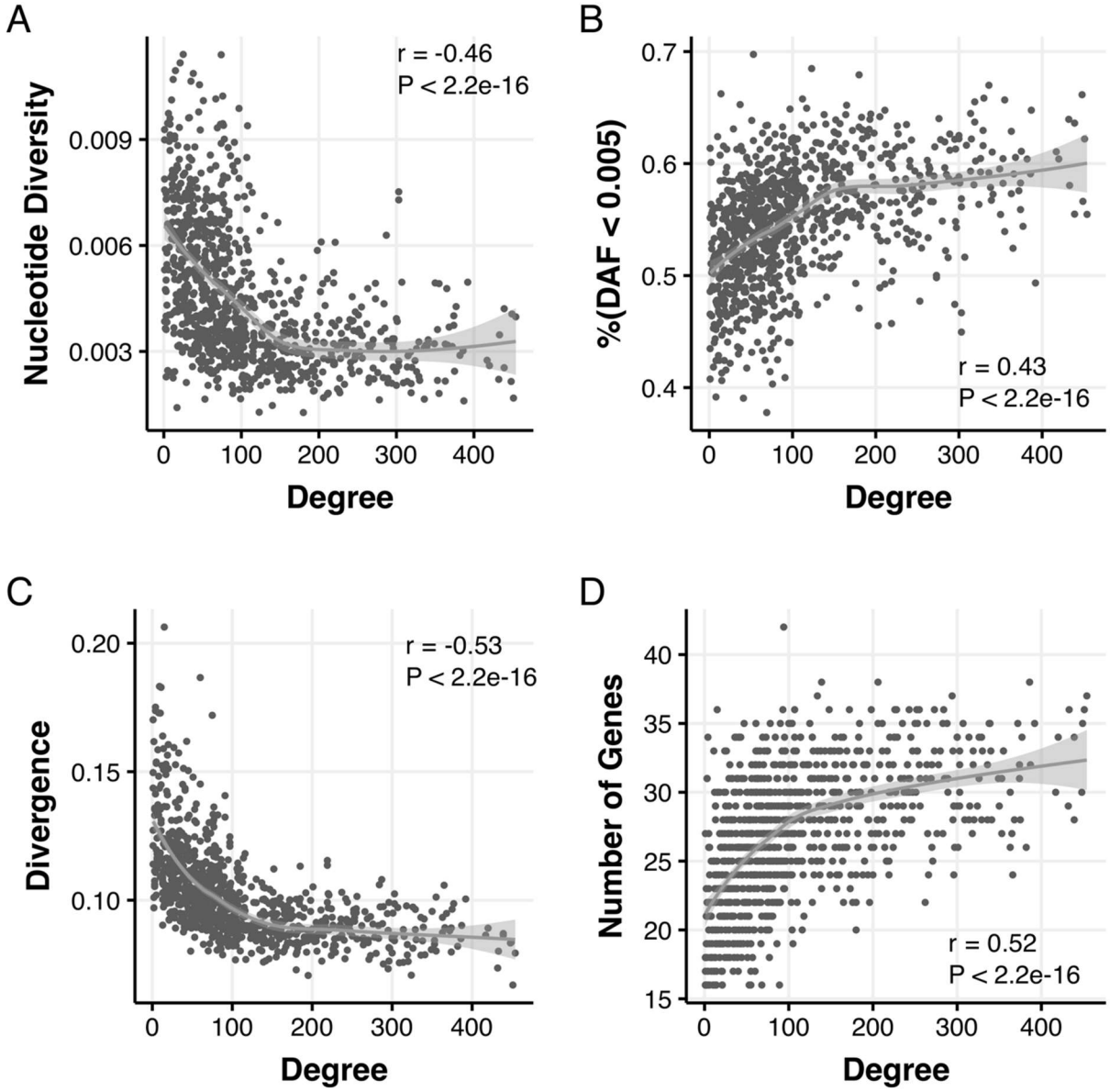
A
Nucleotide Diversity
0.009
0.006
0.003
r = -0.46
P < 2.2e-16
0
100
200
300
400
Degree
B
%(DAF < 0.005)
0.7
0.6
0.5
0.4
r = 0.43
P < 2.2e-16
0
100
200
300
400
Degree
C
Divergence
0.20
0.15
0.10
r = -0.53
P < 2.2e-16
0
100
200
300
400
Degree
D
Number of Genes
40
35
30
25
20
15
r = 0.52
P < 2.2e-16
0
100
200
300
400
Degree

Figure 2.

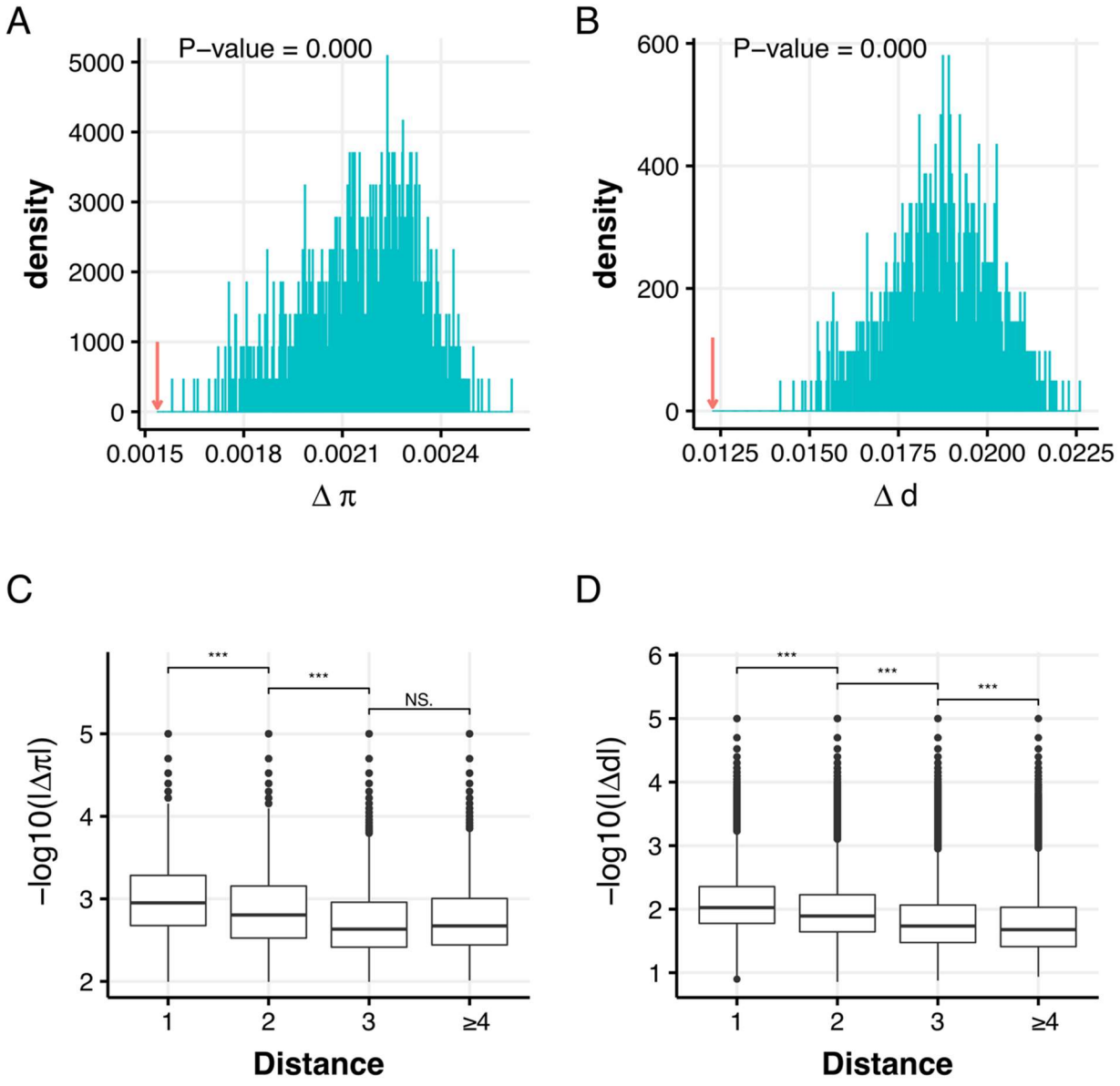
A
P−value = 0.000
density
5000
4000
3000
2000
1000
0
0.0015
0.0018
0.0021
0.0024
Δ π
B
P−value = 0.000
density
600
400
200
0
0.0125
0.0150
0.0175
0.0200
0.0225
Δ d
C
***
***
NS.
−log10(|Δπ|)
5
4
3
2
1
2
3
≥4
Distance
D
***
***
***
−log10(|Δd|)
6
5
4
3
2
1
2
3
≥4
Distance

Figure 3.

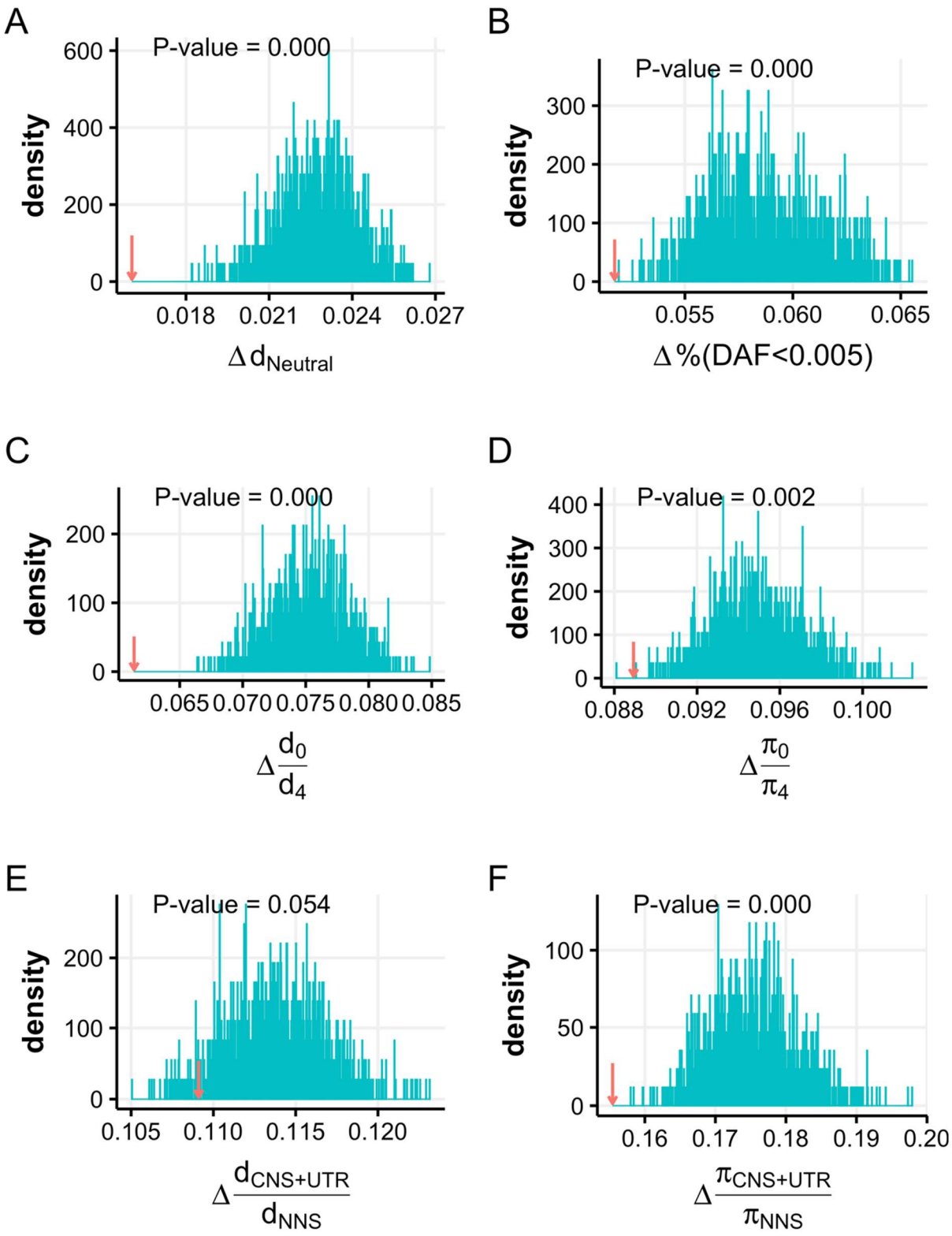
A
P-value = 0.000
density
600
400
200
0
0.018
0.021
0.024
0.027
Δ d_Neutral
B
P-value = 0.000
density
300
200
100
0
0.055
0.060
0.065
Δ %(DAF<0.005)
C
P-value = 0.000
density
200
100
0
0.065 0.070 0.075 0.080 0.085
Δ d0/d4
D
P-value = 0.002
density
400
300
200
100
0
0.088
0.092
0.096
0.100
Δ π0/π4
E
P-value = 0.054
density
200
100
0
0.105
0.110
0.115
0.120
Δ dCNS+UTR/dNNS
F
P-value = 0.000
density
100
50
0
0.16
0.17
0.18
0.19
0.20
Δ πCNS+UTR/πNNS

Figure 4.

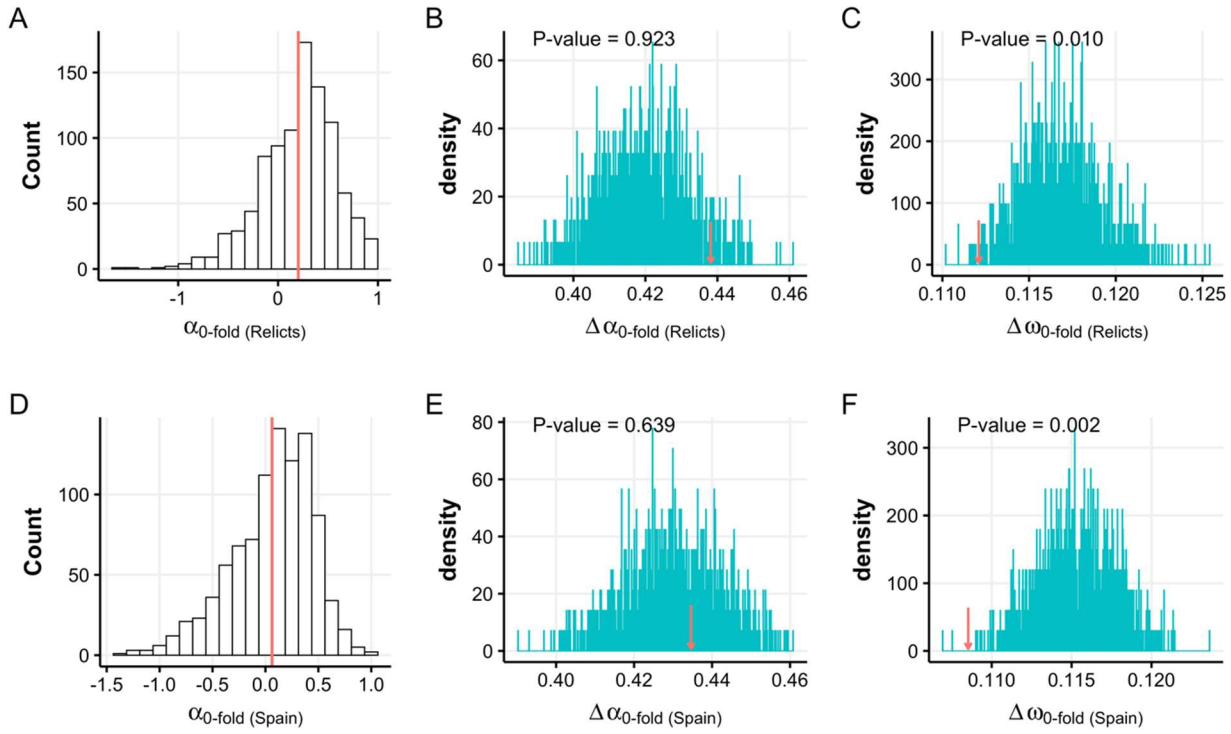
A
Count
150
100
50
0
-1
0
1
$\alpha_{0\text{-fold (Relicts)}}$
B
P-value = 0.923
density
60
40
20
0
0.40
0.42
0.44
0.46
$\Delta\alpha_{0\text{-fold (Relicts)}}$
C
P-value = 0.010
density
300
200
100
0
0.110
0.115
0.120
0.125
$\Delta\omega_{0\text{-fold (Relicts)}}$
D
Count
100
50
0
-1.5
-1.0
-0.5
0.0
0.5
1.0
$\alpha_{0\text{-fold (Spain)}}$
E
P-value = 0.639
density
80
60
40
20
0
0.40
0.42
0.44
0.46
$\Delta\alpha_{0\text{-fold (Spain)}}$
F
P-value = 0.002
density
300
200
100
0
0.110
0.115
0.120
$\Delta\omega_{0\text{-fold (Spain)}}$

Figure 5.

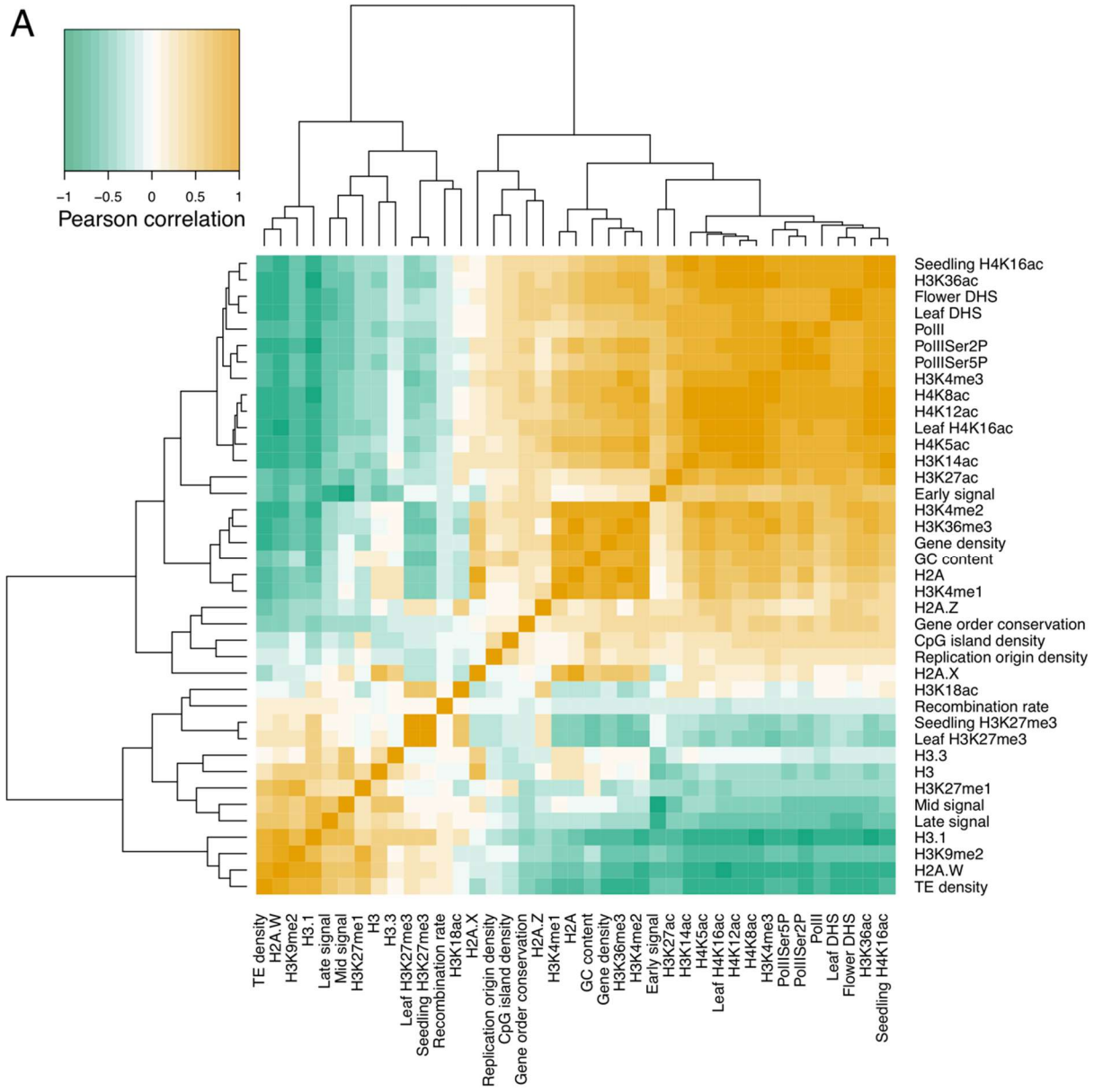
A
−1
−0.5
0
0.5
1
Pearson correlation
Seedling H4K16ac
H3K36ac
Flower DHS
Leaf DHS
PolII
PolIISer2P
PolIISer5P
H3K4me3
H4K8ac
H4K12ac
Leaf H4K16ac
H4K5ac
H3K14ac
H3K27ac
Early signal
H3K4me2
H3K36me3
Gene density
GC content
H2A
H3K4me1
H2A.Z
Gene order conservation
CpG island density
Replication origin density
H2A.X
H3K18ac
Recombination rate
Seedling H3K27me3
Leaf H3K27me3
H3.3
H3
H3K27me1
Mid signal
Late signal
H3.1
H3K9me2
H2A.W
TE density
TE density
H2A.W
H3K9me2
H3.1
Late signal
Mid signal
H3K27me1
H3
H3.3
Leaf H3K27me3
Seedling H3K27me3
Recombination rate
H3K18ac
H2A.X
Replication origin density
CpG island density
Gene order conservation
H2A.Z
H3K4me1
H2A
GC content
Gene density
H3K36me3
H3K4me2
Early signal
H3K27ac
H3K14ac
H4K5ac
Leaf H4K16ac
H4K12ac
H4K8ac
H3K4me3
PolIISer5P
PolIISer2P
PolII
Leaf DHS
Flower DHS
H3K36ac
Seedling H4K16ac

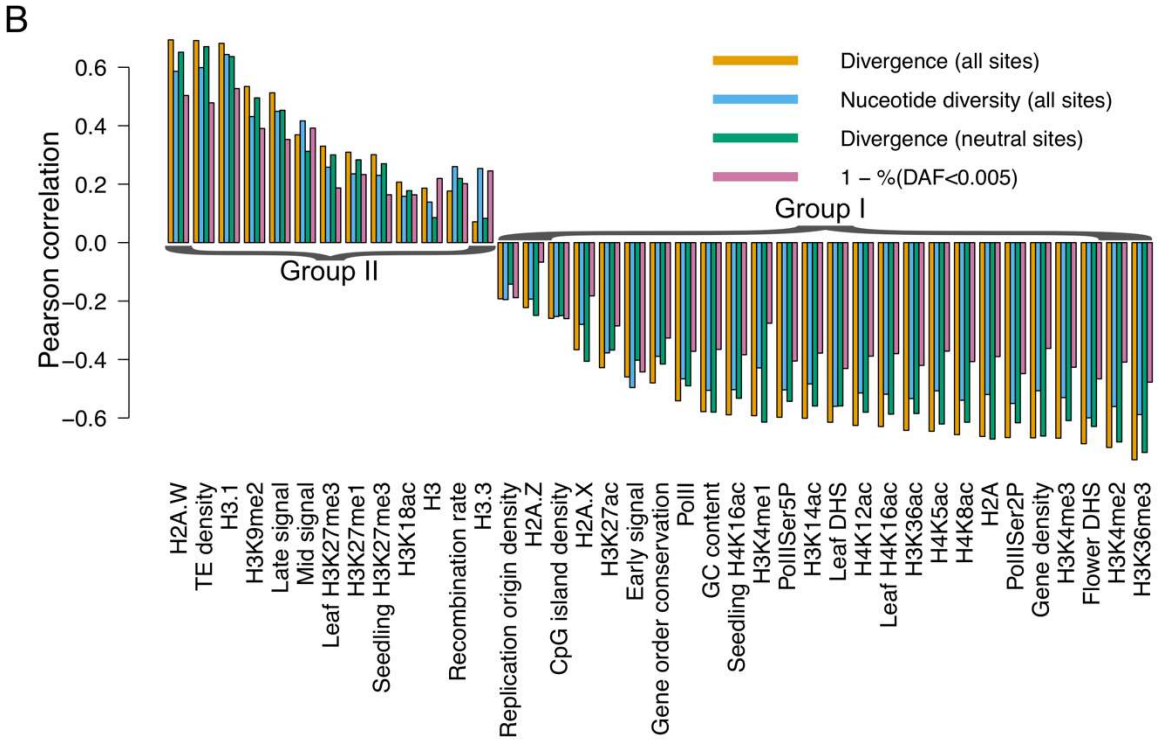
B
Pearson correlation
0.6
0.4
0.2
0.0
−0.2
−0.4
−0.6
Divergence (all sites)
Nuceotide diversity (all sites)
Divergence (neutral sites)
1 − %(DAF<0.005)
Group I
Group II
H2A.W
TE density
H3.1
H3K9me2
Late signal
Mid signal
Leaf H3K27me3
H3K27me1
Seedling H3K27me3
H3K18ac
H3
Recombination rate
H3.3
Replication origin density
H2A.Z
CpG island density
H2A.X
H3K27ac
Early signal
Gene order conservation
PolII
GC content
Seedling H4K16ac
H3K4me1
PolIISer5P
H3K14ac
Leaf DHS
H4K12ac
Leaf H4K16ac
H3K36ac
H4K5ac
H4K8ac
H2A
PolIISer2P
Gene density
H3K4me3
Flower DHS
H3K4me2
H3K36me3

C

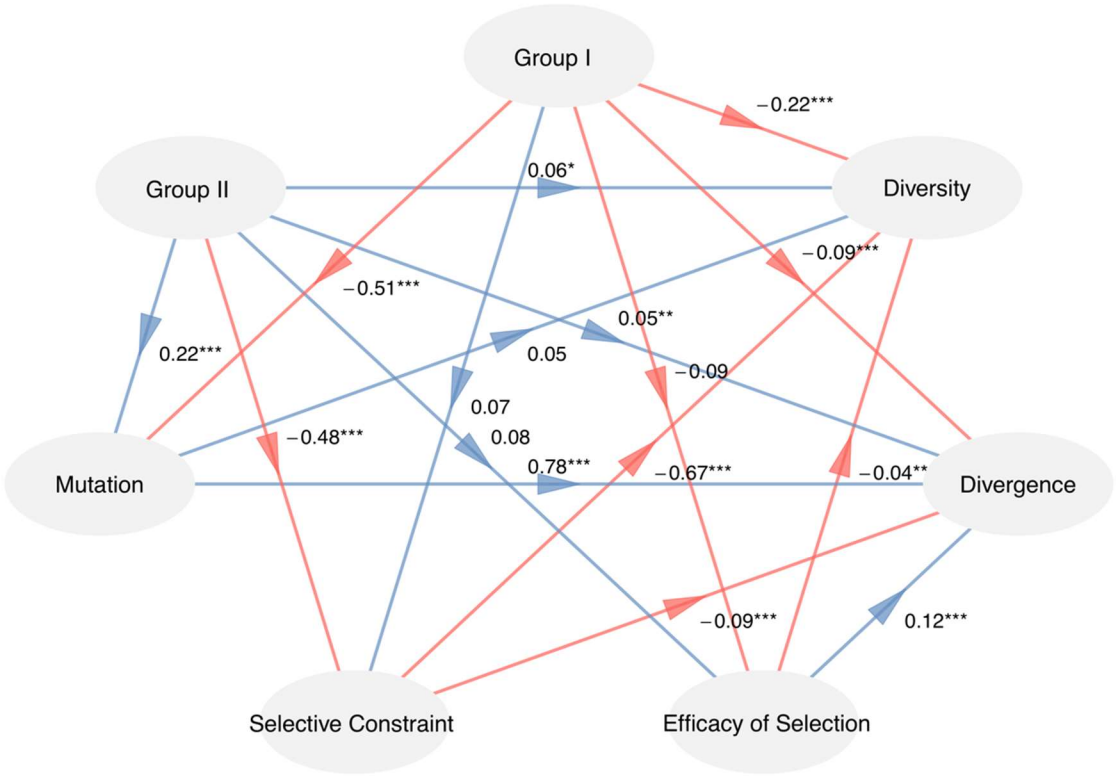
Group I
Group II
Diversity
Mutation
Divergence
Selective Constraint
Efficacy of Selection
−0.22***
0.06*
−0.09***
−0.51***
0.05**
0.22***
0.05
−0.09
0.07
0.08
−0.48***
0.78***
−0.67***
−0.04**
−0.09***
0.12***

Figure 6.

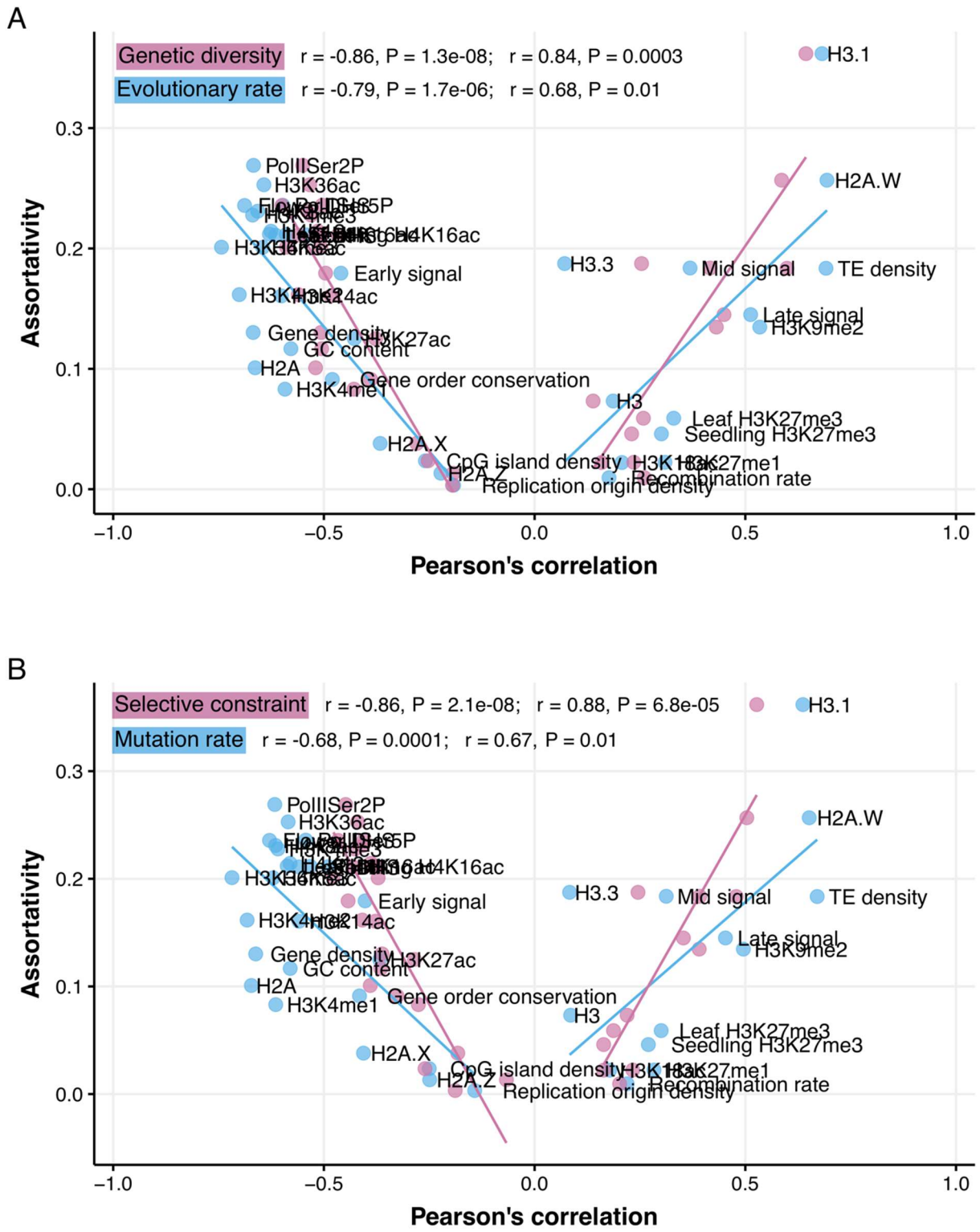
A
Genetic diversity r = -0.86, P = 1.3e-08; r = 0.84, P = 0.0003
Evolutionary rate r = -0.79, P = 1.7e-06; r = 0.68, P = 0.01
Assortativity
Pearson's correlation
H3.1
PolIISer2P
H3K36ac
H2A.W
H3.3
Mid signal
TE density
Early signal
Late signal
H3K9me2
Gene density
GC content
H3K27ac
H2A
Gene order conservation
H3K4me1
H3
Leaf H3K27me3
Seedling H3K27me3
H2A.X
CpG island density
H2A.Z
Replication origin density
Recombination rate
B
Selective constraint r = -0.86, P = 2.1e-08; r = 0.88, P = 6.8e-05
Mutation rate r = -0.68, P = 0.0001; r = 0.67, P = 0.01
Assortativity
Pearson's correlation
H3.1
PolIISer2P
H3K36ac
H2A.W
H3.3
Mid signal
TE density
Early signal
Late signal
H3K9me2
Gene density
GC content
H3K27ac
H2A
Gene order conservation
H3K4me1
H3
Leaf H3K27me3
Seedling H3K27me3
H2A.X
CpG island density
H2A.Z
Replication origin density
Recombination rate